

Adsorption of H₂, O₂, H₂O, OH and H on monolayer MoS₂

F Ferreira¹, A Carvalho², Í J M Moura³, J Coutinho⁴ and R M Ribeiro¹

¹ Centro de Física and Departamento de Física and QuantaLab, Universidade do Minho, Campus de Gualtar, Braga 4710-057, Portugal

²Centre for Advanced 2D Materials and Graphene Research Centre, National University of Singapore, Singapore 117542, Singapore

E-mail: ricardo@fisica.uminho.pt

³Centro de Física and Departamento de Física and QuantaLab, Universidade do Minho, Campus de Gualtar, Braga 4710-057, Portugal; CAPES Foundation, Ministry of Education of Brazil, Brasília – DF, 70040-020, Brazil.

⁴Department of Physics and I3N, University of Aveiro, Campus Santiago, 3810-193 Aveiro, Portugal.

Abstract. Hydrogen and hydrogen-containing gases are commonly used as reductants in chemical vapor deposition (CVD) growth of MoS₂. Here, we consider the defects resulting from the presence of hydrogen during growth and the resulting electronically active defects. In particular, we find that the interstitial hydrogen defect is a negative- U center with amphoteric donor and acceptor properties. Additionally, we consider the effects of the interaction with water and oxygen. The defects are analysed using density functional theory calculations.

PACS numbers: 68.43.Bc, 68.43.Fg, 74.20.Pq

MoS₂, Adsorption, DFT

1. Introduction

The transition metal dichalcogenide MoS_2 is amongst the most studied two-dimensional semiconductors, due to its optical bandgap in the visible range (1.8 eV), and the possibility of selective optical excitation of spin and valley states with potential applications to information processing.

In recent years, efforts have been made to develop cheap and scalable methods to grow 2D materials having in view the possibility of industrial device production. The chemical vapor deposition (CVD) approach is one of the most promising for the production of graphene, MoS_2 and other chalcogenides, boron nitride, amongst others. Recently, several groups have produced MoS_2 mono or few layers using CVD.[Lee and et al.(2012), Kim and et al.(2015), Kim and et al.(2016), Mohapatra and et al.(2016)] The operation parameters of the method, including precursors, growth atmosphere, etc., vary, and are critical for the crystallinity and purity of the material grown. MoS_2 is typically produced by reduction of MoO_3 or Mo by sulfurization with sulfur or H_2S . [Kim and et al.(2016)] Different from the growth of graphene, the addition of H_2 to the MoS_2 growth atmosphere was found to inhibit the thermal-induced etching process during film growth and promote desulfurization and, in large concentrations, to damage the continuity of the film.[Li(2015)] Apart from direct addition of H_2 or H_2S , hydrogen can also be inadvertently incorporated during the various processing steps to which the film is submitted from growth to device fabrication.

Atmospheric oxygen is normally believed to heal vacancies and other defects resulting from sulphur deficiency in MoS_2 . [Ma(2016)] Oxygen-assisted CVD growth has also been reported to result in improved domain growth and crystallinity.[Chen(2015)] However, if the material is exposed to oxygen plasma together with hydrogen treatment, reactive sites are introduced instead.[Ye(2016)] However, little is known about the role of oxygen and hydrogen defects in CVD MoS_2 , as these small elements escape detection in atomically resolved scanning electron microscopy or scanning tunneling microscopy. Clearly, however, the structure of the defects involved and the respective reactions need to be better described in order for the reactivity and electronic character of the resulting MoS_2 material to be controllable, to produce either chemically active substrates for catalysis applications or highly crystalline, passivated semiconductors for electronic and optoelectronic applications.

In this work, we do non colinear density functional theory with spin-orbit calculations to study the adsorption of H_2 , O_2 , OH , H_2O molecules and atomic H on the MoS_2 monolayer. The spin-orbit coupling is needed to obtain the correct electronic structure, and has little effect in the interaction between the substrate and the adsorbants. In Section 2 we describe the method. In Section 3 we present the results and discuss them, starting by the configurations the molecules adopt on the surface and its energetics. Then we look at the resulting electronic structures.

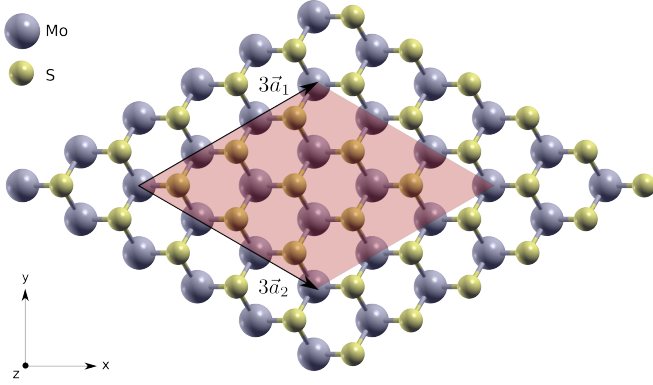


Figure 1. (Color online) Monolayer MoS_2 . The red shadow region is the area of the supercell considered; $3\vec{a}_1$ and $3\vec{a}_2$ are the lattice vectors of the supercell.

2. Method

Calculations were performed using non collinear density-functional theory (DFT) with spin-orbit interaction with the open source software QUANTUM ESPRESSO.[Giannozzi and et al.(2009)] The exchange-correlation functional used was the generalized gradient approximation of Perdew-Burke-Ernzerhof (GGA-PBE).[Perdew and et al.(1996)] We included a van der Waals interaction through the semi-empiric dispersion term of Grimme.[Grimme(2006), Barone and et al.(2009)] A cut-off energy of 50 Ry is used for all configurations, except for configurations involving oxygen, where 80 Ry was used. These cut-off energies were determined after a convergence analysis. The integrations over the Brillouin-zone (BZ) were performed using scheme proposed by Monkhorst-Pack [Monkhorst and Pack(1976)] with a grid of $3 \times 3 \times 1$ \mathbf{k} points. Norm conserving pseudopotentials generated with fully relativistic calculations including spin-orbit interaction were used after extensive tests of their quality.

A supercell is used to avoid the interaction of the molecules with its periodic images (Figure 1) and it is separated from the adjacent layer by a distance of 45 bohr to prevent interlayer interactions. The optimized lattice constant of monolayer MoS_2 is $a = 3.24 \text{ \AA}$. During the structure optimization only the adsorbed molecule and the sulfur atoms near the molecule were allowed to move, in order to save computational effort. The convergence threshold was 10^{-3} for all the components of all the forces (in atomic units) plus 10^{-7} for the total energy of the system (also in atomic units). We verified that these criteria allow a precision of the order of 0.0006 bohr in the relaxed positions, which is enough for our purposes.

The Brillouin-zone integrations involved in calculating the systems' electronic density of states and optical conductivity were performed with a denser \mathbf{k} point grid of $50 \times 50 \times 1$ \mathbf{k} points and using a gaussian broadening of 0.05 Ry.

For the specific case of hydrogen defects in MoS_2 we calculated the depth of carrier traps, namely donor and acceptor transitions, by adding or removing electrons to the defective supercell. This was done concurrently with the inclusion of a compensating

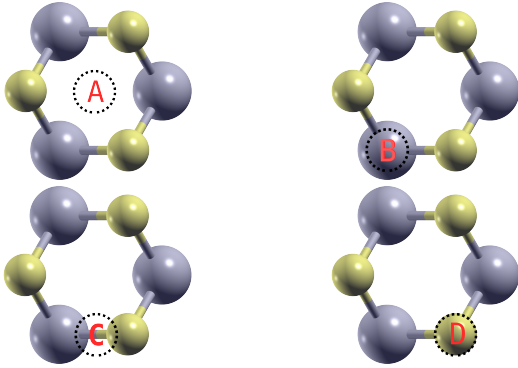


Figure 2. (Color online) Initial sites for the molecules on the monolayer MoS_2 . At site A the adsorbant is on the center of the hexagon, at site B on top of the Mo, at site C on top of the bound between Mo and S and at site D on top of S.




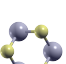
uniform charge density across the supercell, so that the integrated charge per cell was effectively zero. Although this is a standard approach, total energies are affected by spurious Coulomb interactions between the artificial array of charged defects. We mitigated these effects by correcting the total energy of charged cells using the method proposed by Freysoldt, Neugebauer, and Van de Walle,[Freysoldt and et al.(2009)] which was recently generalized for anisotropic materials.[Kumagai and Oba(2014)] Accordingly, the Coulomb interaction between charged defects within the MoS_2 layer and across vacuum-separated layers was considered to be screened by dielectric constants $\epsilon_{\parallel} = 4.8$ and $\epsilon_{\perp} = 1$, respectively. The former value was previously obtained theoretically.[Kumar and Ahluwalia(2012)]

3. Results and Discussion

3.1. Configurations of adsorbants on MoS_2 monolayer

To determine the most favorable configurations of the adsorbants on the MoS_2 monolayer we placed them on different initial sites of the supercell, and three (four in the case of water and OH) different initial orientations. The chosen sites can be seen in figure 2 and are labeled A, B, C and D. For each configuration we let the system relax, so it reconstructs until it reaches an energy minimum. We obtained several metastable configurations for the adsorbants. Table 1 shows the energetics and orientations of the adsorbants in a schematic way in the four positions considered. The adsorption energy was calculated by subtracting to the total energy of the system the sum of the energy of the substrate without adsorbant and the energy of the isolated molecule. Then, for the lowest energy final configuration, we give more details in Table 2, like distances and angles between the adsorbants and the atoms in MoS_2 .

Table 1. Adsorption energies (E_{ads}) and orientations for the adsorbants in the four reference positions. The first column shows the positions already shown in Figure 2. The third column shows the binding energies for the adsorbants of the second column at the site given in the first. The last column shows the orientation of the axis of the adsorbant: x, y, and z are the directions shown in Figure 1; -z for the OH means H is closer to the MoS_2 surface in a z oriented radical; xz means a line about 45° between the x and the z axis and similar definitions for xy and yz. Concerning the water molecule, the oxygen atom is always further away from the MoS_2 surface than the hydrogen atoms; $\parallel y$ means the hydrogen atoms are aligned parallel to the y axis, while the plane of the molecule makes an angle with the normal to the substrate; $\parallel yz$ means the same hydrogen atoms alignment but the plane of the molecule is parallel to the yz plane; in bold are the energies for the most stable positions, also shown in Table 2. H_2 and OH have no stable position in C.

Position	Adsorbant	E_{ads} (eV)	Orientation
A 	H_2	-0.520	z
	O_2	-0.778	xz
	OH	-1.045	-z
	H_2O	-0.795	$\parallel y$
B 	H_2	-0.523	z
	O_2	-0.784	y
	OH	-1.275	z
	H_2O	-0.794	$\parallel y$
C 	H_2	-	-
	O_2	-0.771	xz
	OH	-	-
	H_2O	-0.777	$\parallel yz$
D 	H_2	-0.514	z
	O_2	-0.756	xz
	OH	-1.874	xz
	H_2O	-0.794	$\parallel yz$

The configurations with the lowest adsorption energy corresponding to the most favorable configurations for each adsorbant are shown in Figure 3.

We first consider the physisorbed molecules, H_2 , O_2 and H_2O , which have in common being bounded to the MoS_2 monolayer by distances larger than 4.5 Bohr. H_2 showed very small differences in energies (less than $k_B T \simeq 0.0256$) for the different sites and orientations. The lowest energy site found had H_2 on top of Mo (site B) with an orientation perpendicular to the MoS_2 surface, as shown in Figure 3(a). All other sites were also found to be stable except C.

The O_2 molecule showed a clear preference to be positioned on top of Mo with an orientation parallel to the MoS_2 surface as shown in Figure 3(b). An orientation perpendicular to the surface is unfavorable, but the difference in energy for different

Table 2. Adsorption energies (E_{ads}) and fully relaxed distances for the adsorbants on the top of the MoS_2 monolayer, for the lowest energy configuration. For the meaning of distances and angles, refer to figures 3 and 4. For the site, refer to figure 2.

Molecule	Site	E_{ads} (eV)	d_1 (bohr)	d_2 (bohr)	d_3 (bohr)	d_4 (bohr)	α
H_2	B	-0.52	5.04	8.04	1.42		
O_2	B	-0.78	5.61	8.61	2.33		
H_2O	A	-0.79	4.72	7.72	1.84		48.1°
HO	D	-1.87	3.14	6.14	1.86	3.27	22.0°
H	A	-2.60	3.03	3.62			

Table 3. Relative energies of atomic hydrogen in monolayer MoS_2 , for different charge states (eV). For the configuration labelling, refer to figure 4. For the site, refer to figure 2.

configuration	-	0	+
C	0.35	0.08	0.71
A	0.37	0.00	0.00
A'	0.00	0.14	relaxes to A

orientations parallel to the surface is smaller than 10 meV.

The H_2O molecule in contrast shows preference for the center of the hexagon (site A). But, contrary to the previous molecules, there are configurations with almost the same energy (a difference smaller than 1 meV) on sites B and D, although with different orientations. Its most favorable orientation is not totally parallel to MoS_2 surface, but making an angle of 48°, as can be seen in Figure 3(d). A position where the oxygen is closer to the surface than the hydrogen atoms is never energetically favorable.

Another possibility is that water is chemisorbed, rather than physisorbed on the surface, dissociating into a OH radical and a H atom. The preferred orientation of the OH radical is shown on Figure 3(c); it forms a bond to the sulfur atom through the oxygen, no matter the original position, and the H atom is oriented towards the center of the hexagon. Therefore, the OH group has much lower mobility on the MoS_2 monolayer than physisorbed species, since the OH radical effectively binds to the sulfur atom, forming a chemical covalent bond with the MoS_2 monolayer.

The hydrogen atom or proton occupies preferably the A position of the lattice. We considered two other alternative locations, shown in Figure 4: a position near the bond center (C), and a position on the top of A, but displaced outwards from the layer (A'). Even though both of these competing positions are stable in the neutral charge state, they are respectively 0.08 and 0.14 eV higher in energy than the A position for the neutral charge state (Table 3). This is also the most stable position in the negative charge state. In the positive charge state, however, A' is more stable, as hydrogen prefers to sit closer to the more electronegative S atoms.

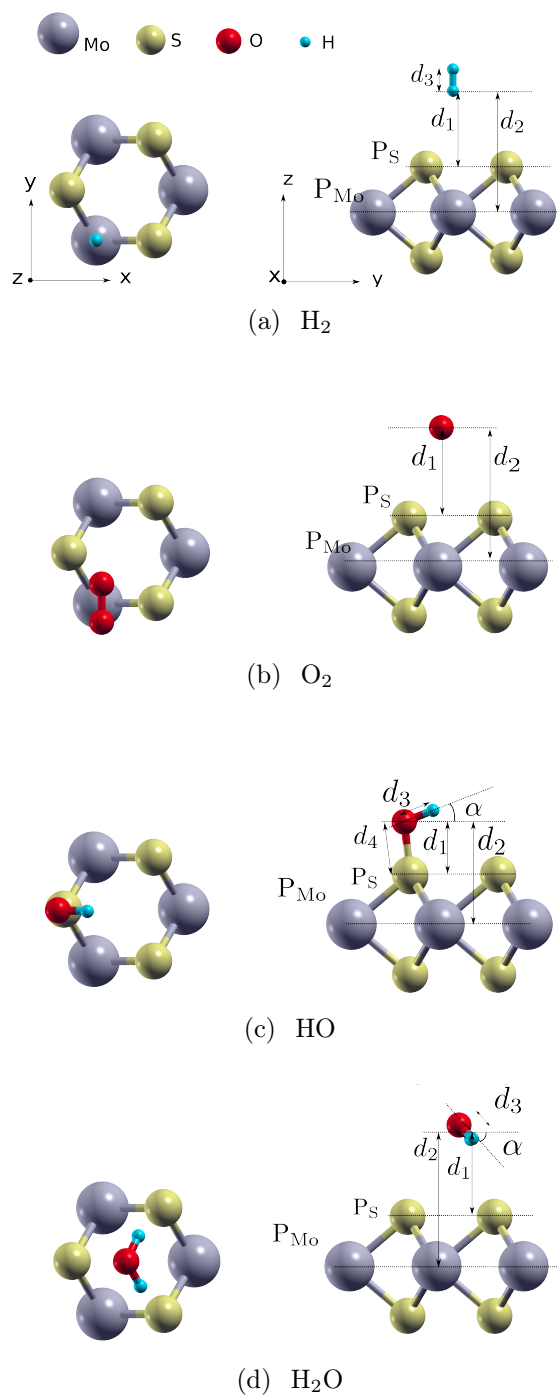


Figure 3. (Color online) Monolayer MoS_2 with adsorbants on the most favorable position. Left: Top view; Right: side view. On the right side, the distances and angles referred on Table 2 are shown. P_S and P_{Mo} are the sulfur and molybdenum planes, respectively.

3.2. Electronic states

After obtaining the most stable configuration for each adsorbant, we determined the electronic structure of these systems. The band diagrams were obtained by going

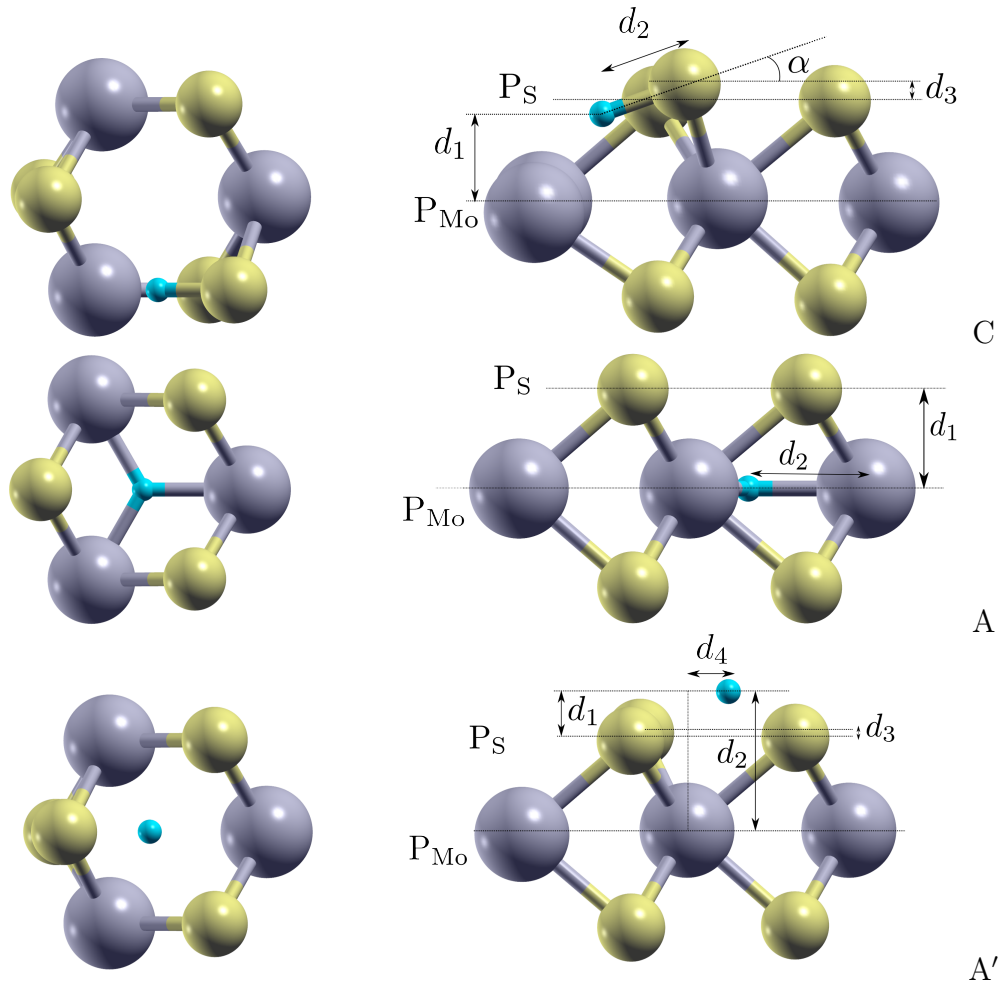


Figure 4. (Color online) Stable configurations of the hydrogen impurity in monolayer MoS_2 . The top figure shows configuration C, the middle shows configuration A and the bottom shows configuration A'. The distances indicated are given in Table 2.

from the extreme of the Brillouin Zone (BZ) of the supercell on the y-axis direction of the reciprocal space, to the Γ point, and then towards the extreme of the BZ of the supercell on the x-axis direction of the reciprocal space. This trajectory on the reciprocal space ensures that we pass on the most relevant high symmetry points of the BZ. The particular size of the supercell chosen makes the K-point of the MoS_2 monolayer unit cell fold on the top of the Γ -point (see Figure 5). The top of the valence band is on the K-point (corresponding to the so called A peak of the absorption spectra); the next band is at the Γ -point, which has an energy between the spin-orbit split bands at the K-point (the blue band of Figure 5); the third band is again at the K-point (corresponding to the so called B peak of the absorption spectra).

Figure 6 (left) shows the band structures of pristine MoS_2 monolayer and MoS_2 monolayer with adsorbed H_2 . When adsorbed, the H_2 molecule has little influence on the electronic states of the MoS_2 monolayer near the gap. It can be seen in Figure 6 (left) that there are no noticeable changes in the valence and conduction bands, and

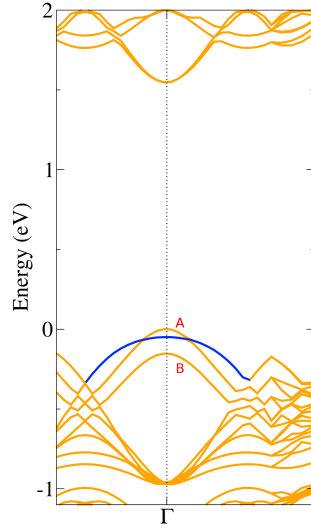


Figure 5. (Color online) Band structure of the MoS_2 monolayer supercell. The folding of the bands turns the K-point on the top of the Γ -point. A and B denote the spin-orbit split bands at the K-point, while the blue band is the band at the Γ -point.

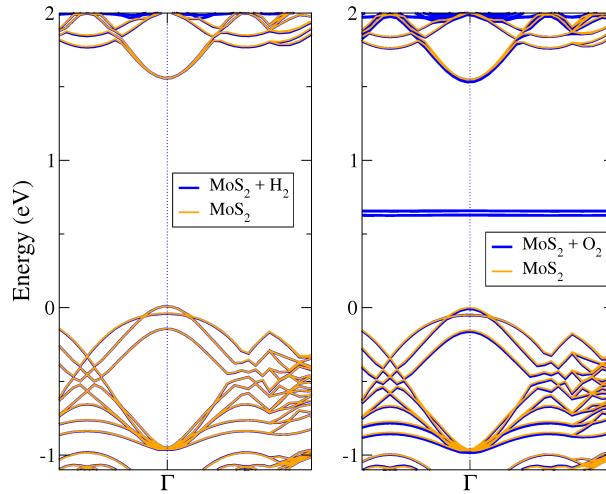


Figure 6. (Color online) Band structure of the pristine MoS_2 monolayer (orange) and of MoS_2 monolayer with adsorbed H_2 (left) and with adsorbed O_2 (right). Band structures are overlapped in order to make the differences noticeable.

the gap remains unchanged. The only change we can observe is a deep state with an energy of approximately -4.5 eV, which is too far from the gap to have relevance on MoS_2 electronic properties.

In the other hand, the O_2 molecule induced states in the gap, as can be seen in Figure 6 (right). Although it is hard to distinguish in Figure 6, there are four states in the gap, two of them occupied and the other two unoccupied, non-degenerated but with very close energies. The energy difference between the occupied and unoccupied states is 0.03 eV. These states may play a role on the absorption spectrum and on scattering of carriers.

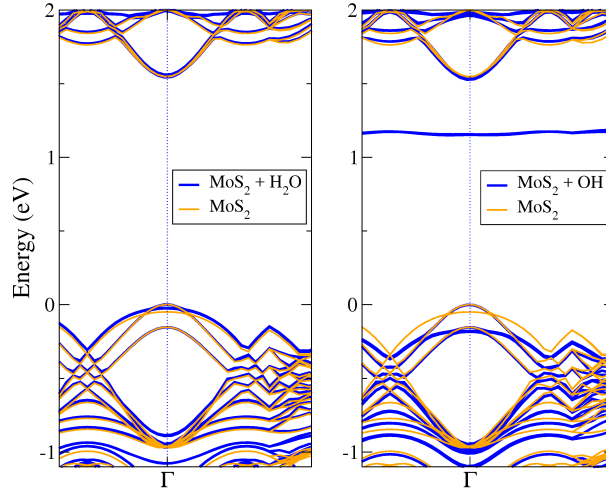


Figure 7. (Color online) Band structure of pristine MoS_2 monolayer (orange) and band structure of MoS_2 monolayer with adsorbed OH (left) and with adsorbed H_2O (right). Band structures are overlapped in order to make the differences noticeable.

The H_2O molecule, like H_2 and O_2 , did not change much the band structure of the MoS_2 monolayer. It can be seen in figure 7 (left) the addition of some states below the valence band. The band at the Γ -point increases in energy, getting closer to the top of the valence band; however, there was no change in the gap.

In contrast, the OH and H radicals clearly alter the electronic properties of the MoS_2 monolayer. The bandstructure of OH on MoS_2 is shown in figure 7 (right). Unoccupied defect states are introduced in the gap. Their energies are very close, so we can consider them as quasi-degenerate states. At the Γ point, the wave function of the valence band includes a component p_z of the atomic wavefunctions of sulfur, which strongly interacts with the OH radical. The energy of the valence band at the Γ point decreased approximately by 0.12 eV, and we also observe a small lifting of degeneracy in the same bands. The energy of the quasi degenerate states relative to the valence band is 1.15 eV.

Figure 8 shows the electronic density of states for the systems with adsorbants. The states inside the gap are clearly visible for samples of MoS_2 with OH and O_2 , as expected. These states contribute significantly to the optical properties of these systems, as can be seen in Fig. 9. Figure 9 shows the calculated optical conductivity. The oxygen molecule contributes with both empty and full states inside the MoS_2 gap, leading to transitions both from the valence band to the defect states and from the defects states to the conduction band. This results in the extended absorption band inside the gap that can be seen in Figure 9. The C peak, also known as the band nesting region,[Carvalho and et al.(2013)] is seen to be considerably suppressed by the adsorbed O_2 molecule. The OH radical also affects the C peak.

Atomic H also introduces levels in the gap, and we shall now consider in more detail the charge states of those defects. The ionisation levels, *i.e.* the value of the Fermi energy for which the defect changes its charge state, is

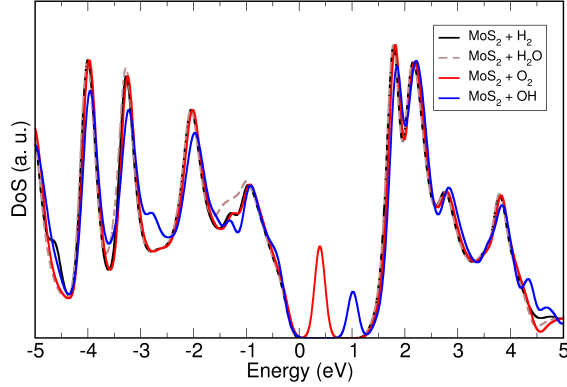


Figure 8. (Color online) Electronic density of states for the systems with adsorbants.

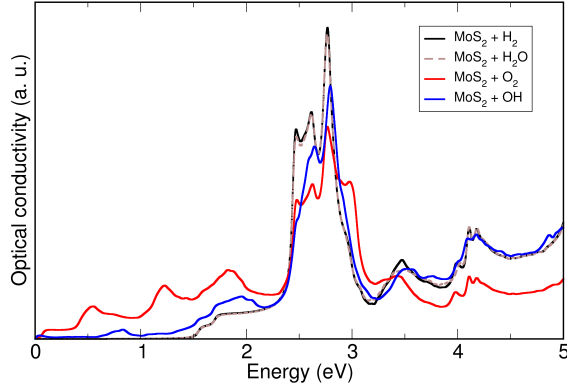


Figure 9. (Color online) Optical conductivity for the systems with adsorbants.

calculated within the marker method,[Coutinho and et al.(2003)] using the perfect supercell as reference. This approach derives from the delta self-consistent (Δ SCF) method,[Hedin and Lundqvist(1970)] where the valence band top is obtained from the ionization energy of a bulk supercell, $E_v = E_{\text{bulk}}(0) - E_{\text{bulk}}(+)$. It can also be demonstrated that when total energies of defective supercells account for periodic charge corrections, the *bulk-marker approach* is equivalent to the *formation energy method* as proposed by Qian, Martin, and Chadi.[Qian and et al.(1988)] They differ only on the definition of the valence band top. In the latter method, E_v is replaced by the highest occupied Kohn-Sham eigenvalue.

Figure 10 shows how the adsorption energy for atomic hydrogen depends on the Fermi energy (E_F). On the vertical axis, E_F can vary within a 1.54 eV wide band gap. Gray areas represent valence band and conduction band energies. The vertical solid line at -2.6 eV stands the adsorption energy of neutral hydrogen at site A (H_A^0), whereas lines with negative and positive slope represent the energy of negatively charged and

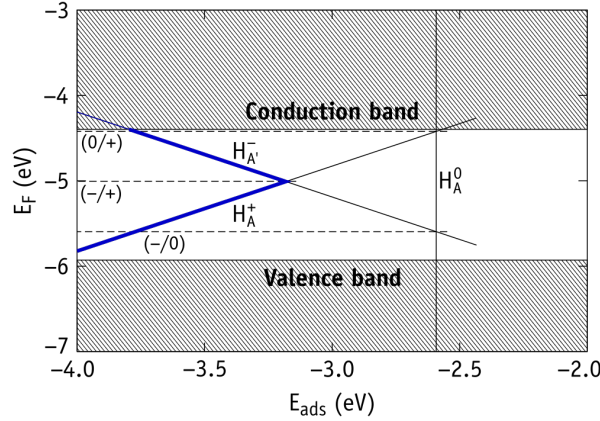


Figure 10. (Color online) Relation between the Fermi level position (E_F) and the adsorption energy (E_{ads}) of atomic hydrogen in monolayer MoS_2 (solid lines). Thick and thin lines represent ground state and metastable (excited) states. The dashed line serves as guidance to the location of the (0/+), (-/0) and (-/+) transitions. See text for further details.

positively charged H at A' and A sites, respectively.

From Figure 10 it becomes clear that hydrogen is an amphoteric impurity – in both n- and p-type materials it may trap majority carriers to become negatively and positively charged, leading to a compensation effect. It is interesting to note that neutral H is metastable irrespectively of the E_F location. The defect can only be found as a proton at site A (H_A^+) or as a hydride atom at the A' site ($H_{A'}^-$). This is emphasized in Figure 10 as thick blue lines, intersecting at the (-/+) transition calculated at $E_v + 0.92$ eV. Hydrogen at site A is a shallow donor with a level edging the conduction band minimum. This explains the small periodic charge correction of only $E_{corr} = -0.04$ eV for this defect. On the other hand, $H_{A'}^-$ has a localized acceptor state, and therefore has a considerably larger charge correction ($E_{corr} = -0.88$ eV).

Our calculations place the donor and acceptor levels of hydrogen at $E_v + 1.51$ eV and $E_v + 0.32$ eV (see upper and lower dashed lines in Figure 10). These levels are metastable and show a negative- U ordering, like atomic H does in many other materials.[Van de Walle and Neugebauer(2003)] Thus, hydrogen is unlikely to be the main source of n-type conductivity often reported in samples not intentionally doped. Our calculations show that as the Fermi energy raises in the gap, H^- will form and compensate any existing shallow donors, including H at site A.

4. Conclusions

The most stable configurations for H_2 , O_2 and H_2O molecules on a MoS_2 monolayer were determined. It was found that only O_2 molecule introduces levels in or close to the bandgap. The most stable configurations for OH radicals and atomic H on a MoS_2 monolayer were also determined. OH radicals form a chemical covalent bond with the MoS_2 monolayer between oxygen atom and sulfur atom, with the hydrogen pointing to

the center of the hexagon. Atomic H tends to sit in the middle of the hexagon.

The influence on electronic properties was also studied. H_2 , O_2 and H_2O did not change significantly the valence and conduction bands of the MoS_2 monolayer. However, the O_2 molecule induced two pairs of quasi-degenerate states in the gap zone, one of the pairs being occupied and the other not. The OH radical changes the valence band at the Γ point lowering its energy and also induces empty states in the gap. The relative stability of the charged states of atomic H were determined and it was found that hydrogen is amphoteric with metastable levels at $E(0/+) = E_v + 1.51$ eV and $E(-/0) = E_v + 0.32$ eV. These show a negative- U ordering, produce a $(-/0)$ thermodynamic transition at $E_v + 0.92$ eV, and therefore hydrogen is able to compensate any deliberate doping.

In summary, O_2 and OH influence the electronic and optical properties of the MoS_2 monolayer. The fact that they induce states in the gap zone changes the electronic properties of the MoS_2 monolayer, and makes this material sensitive to these molecules. Particularly, water dissociation leads to the formation of covalently bonded OH and interstitial H, both of them electrically active. The control of the OH and H charge states via the Fermi level may be used to control the catalysis activity or for the preparation of suitable intermediate steps for further functionalization reactions.

Acknowledgments

R. M. Ribeiro acknowledge support from the European Commission through the project "Graphene-Driven Revolutions in ICT and Beyond" (Ref. No. 696656), and for the financial support by FEDER through the COMPETE2020 Program, project PTDC/FIS-NAN/3668/2014, and the Portuguese Foundation for Science and Technology (FCT) in the framework of the Strategic Financing UID/FIS/04650/2013 and UID/CTM/50025/2013. Í. J. M. Moura gratefully acknowledges CAPES scholarship process n° 99999.001250/2015-09. We gratefully acknowledge that some of the first-principles calculations were carried out on the GRC high-performance computer facilities.

References

- [Lee and et al.(2012)] Y.-H. Lee and et al., *Adv. Mater.* **24**, 2320 (2012).
- [Kim and et al.(2015)] J. H. Kim and et al., *Appl. Phys. Lett.* **106**, 251606 (2015).
- [Kim and et al.(2016)] Y. Kim and et al., *J. Phys.: Condens. Matter* **28**, 184002 (2016).
- [Mohapatra and et al.(2016)] P. K. Mohapatra and et al., *Appl. Phys. Lett.* **108**, 042101 (2016).
- [Li(2015)] X. e. a. Li, *Nanoscale* **7**, pages 8398 (2015).
- [Ma(2016)] D. e. a. Ma, *J. Mater. Chem. C* **4**, pages 7093 (2016).
- [Chen(2015)] W. e. a. Chen, *Journal of the American Chemical Society* **137**, pages 15632 (2015), pMID: 26623946, <http://dx.doi.org/10.1021/jacs.5b10519> .

- [Ye(2016)] G. e. a. Ye, \bibfield journal \bibinfo journal Nano Letters\ \textbf \bibinfo volume 16,\ \bibinfo pages 1097 (\bibinfo year 2016), pMID: 26761422, <http://dx.doi.org/10.1021/acs.nanolett.5b04331> .
- [Giannozzi and et al.(2009)] P. Giannozzi and et al., \bibfield journal \bibinfo journal Journal of Physics: Condensed Matter\ \textbf \bibinfo volume 21,\ \bibinfo pages 395502 (\bibinfo year 2009).
- [Perdew and et al.(1996)] J. P. Perdew and et al., \bibfield journal \bibinfo journal Phys. Rev. Lett.\ \textbf \bibinfo volume 77,\ \bibinfo pages 3865 (\bibinfo year 1996).
- [Grimme(2006)] S. Grimme, J. Comput. Chem. **27**, 1787 (2006).
- [Barone and et al.(2009)] V. Barone and et al., J. Comput. Chem. **30**, 934 (2009).
- [Monkhorst and Pack(1976)] H. J. Monkhorst and J. D. Pack, \bibfield journal \bibinfo journal Phys. Rev. B\ \textbf \bibinfo volume 13,\ \bibinfo pages 5188 (\bibinfo year 1976).
- [Freysoldt and et al.(2009)] C. Freysoldt and et al., Phys. Rev. Lett. **102**, 016402 (2009).
- [Kumagai and Oba(2014)] Y. Kumagai and F. Oba, Phys. Rev. B **89**, 195205 (2014).
- [Kumar and Ahluwalia(2012)] A. Kumar and P. K. Ahluwalia, Materials Chemistry and Physics **135**, 755 (2012).
- [Carvalho and et al.(2013)] A. Carvalho and et al., \bibfield journal \bibinfo journal Phys. Rev. B\ \textbf \bibinfo volume 88,\ \bibinfo pages 115205 (\bibinfo year 2013).
- [Coutinho and et al.(2003)] J. Coutinho and et al., \bibfield journal \bibinfo journal Phys. Rev. B\ \textbf \bibinfo volume 67,\ \bibinfo pages 035205 (\bibinfo year 2003).
- [Hedin and Lundqvist(1970)] L. Hedin and S. Lundqvist, Solid State Physics **23**, 1 (1970).
- [Qian and et al.(1988)] G.-X. Qian and et al., Physical Review B **38**, 7649 (1988).
- [Van de Walle and Neugebauer(2003)] C. G. Van de Walle and J. Neugebauer, Nature **423**, 626 (2003).